Analysis of the Bayesian Gait-State Estimation Problem for Lower-Limb Wearable Robot Sensor Configurations

Roberto Leo Medrano[1], Gray Cortright Thomas[2], and Elliott J. Rouse[1,3], Robert D. Gregg[2,3]

***Abstract*— Many exoskeletons today are primarily tested in controlled, steady-state laboratory conditions that are unrealistic representations of their real-world usage in which walking conditions (*e.g.*, speed, slope, and stride length) change constantly. One potential solution is to detect these changing walking conditions online using Bayesian state estimation to deliver assistance that continuously adapts to the wearer's gait. This paper investigates such an approach *in silico*, aiming to understand 1) which of the various Bayesian filter assumptions best match the problem, and 2) which gait parameters can be feasibly estimated with different combinations of sensors available to different exoskeleton configurations (pelvis, thigh, shank, and/or foot). Our results suggest that the assumptions of the Extended Kalman Filter are well suited to accurately estimate phase, stride frequency, stride length, and ramp inclination with a wide variety of sparse sensor configurations.**

I. Introduction

Lower-limb wearable robots, such as exoskeletons and prostheses, have the potential to transform the mobility of the public. Already, powered exoskeletons have been able to improve the physiological performance of users during locomotion, including reducing the metabolic cost [1]–[5] and muscular effort [6]–[8] below the levels of unassisted walking, while powered prostheses have allowed amputees to regain locomotion ability [9]–[14]. However, these technologies have been largely limited to the controlled conditions of a laboratory. To truly impact society, these technologies must function with the unsteady, transitory gaits that arise in the real world, such as walking at variable speeds and inclines. Measuring these task variables, along with the user's progression through a gait cycle, is difficult to do directly. Recent work has demonstrated success in estimating dynamically changing gaits using implementations of the Bayesian filtering framework [15]–[18]. Thus, a systemic investigation into the fundamental problem of gait state estimation using the Bayesian framework can guide wearable robot controller design and may lead to better estimation of real-world walking conditions.

Gait variation can be represented in multiple ways. The concept of *gait phase* quantifies progression through the gait cycle. A phase variable ranges from 0 at heel strike to 1 at the next ipsilateral heel strike [19]. Its time derivative, phase rate, is not necessarily constant. Recent work in phase-based controllers for powered prostheses and orthoses relies on estimates of phase (and sometimes phase rate) [20]–[28] to handle gait speed variation. To encode other types of task variation, machine learning-based solutions often classify the locomotion task from signal patterns from onboard sensors [10], [24], [28]–[35]. However, such controllers are typically only able to classify tasks within a pre-specified set of categories. Walking tasks have been parameterized by continuous *task variables* such as ground slope or walking speed [36]–[38], but these task variables have only been estimated once per stride in laboratory conditions. New methods for real-time, continuous task estimation are needed to enable seamless adaptation to real-world conditions.

Bayesian filtering allows using noisy measurements to estimate hidden states like gait phase and continuous task variables; this framework is well-suited to discriminate the differences in gait biomechanics between strides to notice changes in the underlying task. For linear systems with Gaussian noise, Bayesian filters are implementable as the classic Kalman filter. However, for nonlinear problems, simplifying assumptions are inevitable [39] with differing levels of assumption strength. The Ensemble Kalman Filter (EnKF) has the weak assumption of a Gaussian state distribution, and uses Monte Carlo methods to calculate the measurement update [40]. The Unscented Kalman Filter (UKF) assumes more, and uses quadrature integration and judiciously chosen points and weights to approximate the nonlinear measurement update [41]. The Extended Kalman Filter (EKF) assumes the most, and trusts a local linearization to perform the nonlinear measurement update.

Recently, Bayesian filtering has been applied to human gait estimation in wearable robotics. Thatte et al. [15] introduced a simple two-state EKF as a robust solution to estimating progression through the stance period using the hip, knee, and ankle angles and velocities from a knee-ankle prosthesis. Stance progress was also estimated using the heel pressure and shank angle of an ankle prosthesis [17]. However, the swing period was handled separately in these two approaches. Researchers were also able to estimate stride length using a twice per step filter update using hip and knee velocities from an exoskeleton [16], but this estimate was not continuously updated. Our own recent work introduced a 4-state EKF to simultaneously estimate stride progress (both stance and swing), stride length, and ground inclination using foot and shank angles/velocities and filtered heel acceleration for an ankle exoskeleton [18]. This simultaneous estimation approach begs the question of which measurements inform which states, which sensors are necessary for successful estimation, and to what extent the other Bayesian filters in the literature reflect

*This work was supported by the National Institute of Child Health & Human Development of the NIH under Award Number R01HD094772. The content is solely the responsibility of the authors and does not necessarily represent the official views of the NIH.

[1]Mechanical Engineering, [2]Electrical and Computer Engineering, [3]Robotics Institute, University of Michigan, Ann Arbor, MI 48109, USA. {leomed,gcthomas,ejrouse,rdgregg}@umich.edu

the non-linearity of gait-state estimation.

In this paper, we A) systematically evaluate different implementations of the Bayesian filter to determine which simplifying assumptions (*i.e.*, those of the EnKF, UKF, or EKF) were best suited to the challenge of gait-state estimation; B) investigate which angular kinematic measurements of the leg segments provide the most information about the underlying gait state, which can inform a minimal realization of sensors on hardware that balances estimation quality with sensor complexity; and C) determine the relationship between sensor configurations and estimation of simplified models of the gait state without ground inclination, stride length, or both. We intend for these results to inform the design of future wearable systems that estimate human gait.

II. Methods

A. Process Model

Bayesian estimation employs a forward model that predicts the dynamic evolution of the measurable link angles according to a hidden gait-state that evolves from its initial conditions according to a dynamic model. We begin by defining the gait-state vector x to be estimated,

$$x(t) = \begin{pmatrix} p(t) & \dot{p}(t) & l(t) & r(t) \end{pmatrix}^T, \tag{1}$$

comprised of phase p, phase rate $\dot{p}$, stride length l, and the ground inclination r. The gait-state at time k evolves to time $k+1$ as

$$x_{k+1} = Fx_k + w_Q, \tag{2}$$

with w_Q distributed as zero-mean Gaussian process noise of covariance Σ_Q and state transition matrix F as

$$F = \begin{bmatrix} 1 & \Delta t & 0 & 0 \\ 0 & 1 & 0 & 0 \\ 0 & 0 & 1 & 0 \\ 0 & 0 & 0 & 1 \end{bmatrix}. \tag{3}$$

This choice of F represents a simple numerical integration of phase rate using the time stride Δt. We model Σ_Q as a diagonal matrix $\mathrm{diag}[\sigma_{11}^2, \sigma_{22}^2, \sigma_{33}^2, \sigma_{44}^2] \times \Delta t$, with σ_{22}, σ_{33}, and σ_{44} being standard deviations for $\dot{p}$, l, and r, respectively. The phase variable p generally has no process noise σ_{11} to represent the noiseless integration of $\dot{p}$. The phase variable p is wrapped within $[0, 1)$ using the modulo operation.

B. Nonlinear Stride Length Transformation

Within walking, there exists an upper limit on a person's stride lengths, which is determined by the length of their legs. Additionally, we can choose to model the smallest possible stride length as 0, as negative stride lengths that could model backwards walking are instead handled by positive stride lengths and negative phase rates. To encode these choices, we model the stride length as the output of an arctangent transformation [19], to which the input is a 'pseudo-stride length' l_p. The arctangent transformation is defined as

$$l(l_p) = \frac{2}{\pi}\mathrm{atan}(\frac{\pi}{2}l_p) + 1. \tag{4}$$

This saturates the stride length output at 2 (meters) and floors it at 0. l_p is allowed to vary freely during EKF estimation. Our state vector x technically contains l_p instead of l, but for a more intuitive understanding of our estimation, we referred to it as containing stride length instead of its 'pseudo' counterpart. We also account for this change of variable when taking partial derivatives; for example, within the Jacobian H in the update step of the EKF, we multiply all partial derivatives with respect to l by $\frac{\partial l}{\partial l_p}$.

C. Measurement Model

In contrast to our simple linear process model, the gait-state uses a non-linear function $h(x)$ to predict both joint angle and angular velocity measurements. The joint angle measurements arise from a regressed gait model $h_{\mathrm{gait}}(x)$ trained on human biomechanical data, while the angular velocity measurements can be estimated using the differentiation chain rule. The gait model $h_{\mathrm{gait}}(x)$ is trained offline, but is evaluated in real-time. The continuous gait model $h_{\mathrm{gait}}(x)$ predicts global foot angle θ_f, global shank angle θ_s, global thigh angle θ_t, and global pelvis angle θ_p (all potentially measurable by sensors on a lower-limb wearable robot), and this function is denoted by

$$\begin{pmatrix} \theta_f(t) \\ \theta_s(t) \\ \theta_t(t) \\ \theta_p(t) \end{pmatrix} = \begin{pmatrix} h_f(x(t)) \\ h_s(x(t)) \\ h_t(x(t)) \\ h_p(x(t)) \end{pmatrix} = h_{\mathrm{gait}}(x(t)). \tag{5}$$

Additionally, given knowledge of the phase rate $\dot{p}$, we can also model the angular velocity of the foot $\dot{\theta}_f$, shank $\dot{\theta}_s$, thigh $\dot{\theta}_t$, and pelvis $\dot{\theta}_p$ using the differentiation chain rule:

$$\begin{bmatrix} \dot{\theta}_f \\ \dot{\theta}_s \\ \dot{\theta}_t \\ \dot{\theta}_p \end{bmatrix} = \begin{bmatrix} \partial\theta_f/\partial p \\ \partial\theta_s/\partial p \\ \partial\theta_t/\partial p \\ \partial\theta_p/\partial p \end{bmatrix} \dot{p} \tag{6}$$

where $\dot{p}$ is the estimate of the phase rate from the prediction stride and the partial derivatives of θ_f, θ_s, θ_t, and θ_p are available analytically from the regressed gait model. Phase substitutes in for stride time when parametrizing the gait cycle. The full observation function is then $h(x) = \begin{bmatrix} \theta_f, \dot{\theta}_f, \theta_s, \dot{\theta}_s, \theta_t, \dot{\theta}_t, \theta_p, \dot{\theta}_p \end{bmatrix}^T$. In a practical implementation, these variables will be measured by a combination of sensors on the system chosen by the researcher. In this investigation, we analyzed the impact of using subsets of this 8x1 vector to drive gait state estimation (*e.g.*, using only shank angle and its velocity).

The gait model $h_{\mathrm{gait}}(x)$ is regressed from labeled training data from a 10-subject able-bodied dataset [36], which contains walking data grouped by strides, over a range of speeds (0.8, 1, and 1.2 m/s) and ramps (-10 to 10 degree inclination in increments of 2.5 degrees). Ground-truth phase, phase rate, stride length, and ground inclination, along with the measurements of the global angles at each condition, are readily available from this dataset. The gait model $h_{\mathrm{gait}}(x)$ takes as input the gait state vector x and outputs the best-fit estimates of the kinematic measurements.

For least-squares regression, $h_{\mathrm{gait}}(x)$ is formulated as

$$h_{\mathrm{gait}}(x) = \phi^T R^T(x), \tag{7}$$

where $\phi \in \mathbf{R}^{144\times 4}$ is a matrix of real-valued model parameters and $R : \mathbf{R}^4 \mapsto \mathbf{R}^{1\times 144}$ is a gait-state-dependent regressor row-vector. The parameters ϕ are chosen to minimize the sum squared error for each equation of the form

$$\begin{pmatrix}\theta_f(t) & \theta_s(t) & \theta_t(t) & \theta_p(t)\end{pmatrix} = R(x(t))\phi, \tag{8}$$

for all times t in the training dataset (treating each instant of each step by each participant in each trial as a separate t).

The definition of $R(x)$ makes extensive use of the Kronecker product, $\otimes$ to construct large row-vectors from smaller row-vectors. To review, the Kronecker product of row-vectors $A \in \mathbf{R}^{1\times N}$ and $B \in \mathbf{R}^{1\times M}$, expressed as $A \otimes B \in \mathbf{R}^{1\times NM}$, is the block row-vector $(a_1 B \quad a_2 B \quad \cdots \quad a_N B)$. In the case of matrices $A \in \mathbf{R}^{n\times N},\ B \in \mathbf{R}^{m\times M}$, this generalizes to

$$A \otimes B = \begin{pmatrix} a_{11}B & a_{12}B & \cdots & a_{1N}B \\ a_{21}B & a_{22}B & \cdots & a_{2N}B \\ \vdots & \vdots & \ddots & \vdots \\ a_{n1}B & a_{n2}B & \cdots & a_{nN}B \end{pmatrix} \in \mathbf{R}^{nm\times NM}. \tag{9}$$

The regressor is defined as

$$R(x) = B_p(p) \otimes \Lambda_r(r) \otimes \Lambda_l(l) \otimes \Lambda_p(p), \tag{10}$$

that is, it combines the effects of the four simpler behaviors such that the final model depends on p, l, and r. The components are as follows:

- $B_p(p)$: The Boolean selector row $\mathbf{R} \mapsto \mathbf{R}^{1\times 4}$,

$$B_p(p) = \begin{cases} (1,0,0,0) & \text{if} \quad 0 \le p \le 0.1, \\ (0,1,0,0) & \text{if} \quad 0.1 < p \le 0.5, \\ (0,0,1,0) & \text{if} \quad 0.5 < p \le 0.65, \\ (0,0,0,1) & \text{if} \quad 0.65 < p \le 1, \end{cases} \tag{11}$$

  which divides the gait phase into four sections. In our gait model, we chose four Bernstein polynomials (see $\Lambda_p(p)$ below) to represent the kinematics; Bernstein bases have an equivalent span to polynomial bases and have previously been useful in gait modelling [36]. The sections were determined by inspection of the nominal biomechanical kinematics in our dataset.
- Λ_r : The ramp angle basis ($\mathbf{R} \mapsto \mathbf{R}^{1\times 3}$) is a second-order polynomial Bernstein basis in ramp angle,

$$\Lambda_r(r) = \begin{pmatrix}(1-r)^2 & 2(1-r)r & r^2\end{pmatrix}, \tag{12}$$

  which allows for continuous adjustment to ground slope.
- Λ_l : The stride length basis ($\mathbf{R} \mapsto \mathbf{R}^{1\times 3}$) is a second-order Bernstein polynomial basis in stride length,

$$\Lambda_l(l) = \begin{pmatrix}(1-l)^2 & 2(1-l)l & l^2\end{pmatrix}, \tag{13}$$

  which allows for kinematic changes associated with stride length.
- Λ_p : The phase-polynomial basis $\mathbf{R} \mapsto \mathbf{R}^{1\times 4}$ is a Bernstein polynomial basis, defined as

$$\Lambda_p(p) = \begin{pmatrix}(1-p)^3 & 3(1-p)^2 p & 3(1-p)p^2 & p^3\end{pmatrix}. \tag{14}$$

D. Measurement Model Constraints

To ensure desirable gait model properties, such as continuity of the function $h_{\text{gait}}(x)$ (the global angle predictions) and realistic behavior with changing stride length, the elements of the parameter matrix ϕ are subject to constraints. To express the C^0 continuity of the model, we require $\lim_{p\to\rho^-} h_{\text{gait}}(x) = \lim_{p\to\rho^+} h_{\text{gait}}(x)$ for all $0 < \rho < 1$ as well as the special wrap-around case where $\lim_{p\to 1^-} h_{\text{gait}}(x) = \lim_{p\to 0^+} h_{\text{gait}}(x)$. This is trivially satisfied everywhere except at $\rho = 0.1,\ 0.5,\ 0.65$, and in the wrap-around case. In these four cases, equality constraints must be satisfied for all possible stride lengths and ramp angles. We express this constraint on ϕ using a matrix equality:

$$\begin{pmatrix} (1\ -1\ 0\ 0) \otimes \Lambda_{\forall r} \otimes \Lambda_{\forall l} \otimes \Lambda_p(0.1) \\ (0\ 1\ -1\ 0) \otimes \Lambda_{\forall r} \otimes \Lambda_{\forall l} \otimes \Lambda_p(0.5) \\ (0\ 0\ 1\ -1) \otimes \Lambda_{\forall r} \otimes \Lambda_{\forall l} \otimes \Lambda_p(0.65) \\ \begin{bmatrix}(0\ 0\ 0\ 1) \otimes \Lambda_{\forall r} \otimes \Lambda_{\forall l} \otimes \Lambda_p(1) \\ -(1\ 0\ 0\ 0) \otimes \Lambda_{\forall r} \otimes \Lambda_{\forall l} \otimes \Lambda_p(0)\end{bmatrix} \end{pmatrix} \phi = 0_{36\times 4}, \tag{15}$$

where

$$\Lambda_{\forall r} = \begin{pmatrix}\Lambda_r(10) \\ \Lambda_r(0) \\ \Lambda_r(-10)\end{pmatrix} \text{ and } \Lambda_{\forall l} = \begin{pmatrix}\Lambda_l(0) \\ \Lambda_l(1) \\ \Lambda_l(2)\end{pmatrix} \tag{16}$$

serve to constrain all parts of the quadratic fits in r and l by specifying three (arbitrary but unique) points of each.

To express the C^1 continuity constraint, we exploit the linearity of the Kronecker product. For almost all p we can express the derivative

$$\frac{dh_{\text{gait}}^T(x)}{dp} = \left[B_p(p) \otimes \Lambda_r(r) \otimes \Lambda_l(l) \otimes \frac{d\Lambda_p(p)}{dp}\right]\phi, \tag{17}$$

since $\frac{dB_p(p)}{dp}$ is zero almost everywhere.

Note that $d\Lambda_p/dp : \mathbf{R} \mapsto \mathbf{R}^{1\times 4}$ is available analytically. The resulting continuity constraint is then

$$\begin{pmatrix} (1\ -1\ 0\ 0) \otimes \Lambda_{\forall r} \otimes \Lambda_{\forall l} \otimes d\Lambda_p/dp(0.1) \\ (0\ 1\ -1\ 0) \otimes \Lambda_{\forall r} \otimes \Lambda_{\forall l} \otimes d\Lambda_p/dp(0.5) \\ (0\ 0\ 1\ -1) \otimes \Lambda_{\forall r} \otimes \Lambda_{\forall l} \otimes d\Lambda_p/dp(.65) \\ \begin{bmatrix}(0\ 0\ 0\ 1) \otimes \Lambda_{\forall r} \otimes \Lambda_{\forall l} \otimes d\Lambda_p/dp(1) \\ -(1\ 0\ 0\ 0) \otimes \Lambda_{\forall r} \otimes \Lambda_{\forall l} \otimes d\Lambda_p/dp(0)\end{bmatrix} \end{pmatrix} \phi = 0_{36\times 4}, \tag{18}$$

simply requiring that the derivatives match on either side of each potential discontinuity in p (for all values of r and l).

To ensure constant-with-phase behavior when stride length is zero, *i.e.*, when the person is standing still, we require

$$\underbrace{I_4}^{\forall\ B_p(p),} \otimes \overbrace{\Lambda_{\forall r} \otimes \Lambda_l(0)}^{\forall r,\text{ if } l=0,} \otimes \overbrace{\begin{pmatrix}\Lambda_p(0) \\ \Lambda_p(\frac{1}{4}) \\ \Lambda_p(\frac{1}{2}) \\ \Lambda_p(\frac{3}{4})\end{pmatrix}}^{\forall\ p} \phi = \overbrace{1_{48\times 1} \otimes \begin{pmatrix}c_1 \\ c_2 \\ c_3 \\ c_4\end{pmatrix}^T}^{\text{angles are constant}}. \tag{19}$$

The constraint takes a form similar to the Kronecker construction of the regressor, but where the regressor has $B_p(p)$, the constraint uses an identity matrix. The purpose of this is to expand the row dimension of the constraint so that it applies to any of the four possible cases for $B_p(p)$. Similarly, where the regressor has $\Lambda_p(p)$, the constraint has a block

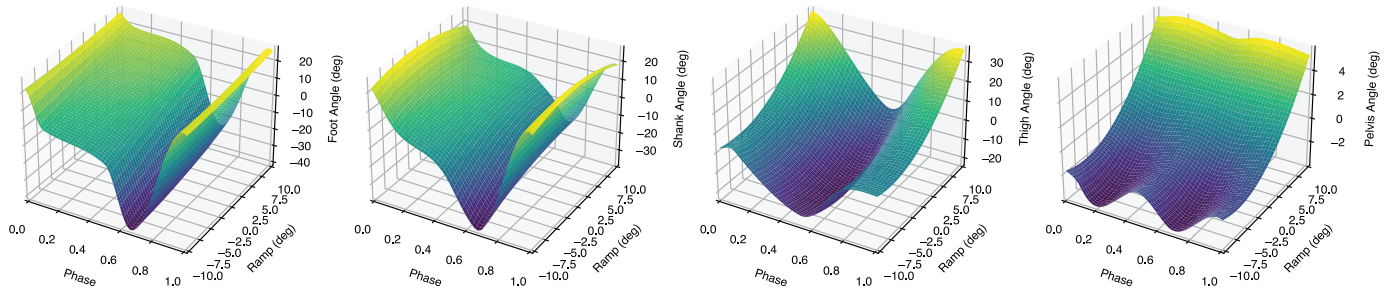

Fig. 1. The regressed continuous gait models for θ_f, θ_s, θ_t, and θ_p, left to right respectively. As each model depends on three input variables (p, l, and r) and has one output variable (θ_f, θ_s, θ_t, or θ_p), the models reside fully in 4D-space and are thus difficult to plot. In this figure, the models are plotted over phase and ramp (with stride length constant at 1 meter).

matrix that constrains the polynomial at four points (enough to ensure the third-order polynomial expression is equal to a constant everywhere). Taken together, these two components of the constraint equation force all four 3rd-order parts of the piecewise polynomial $\Lambda([p, \dot{p}, l = 0, r = 0]^T)\phi$ to be constant for all the measured kinematics. Any four unique phase points could replace the constants $0, \frac{1}{4}, \frac{1}{2}, \frac{3}{4}$ and achieve the same effect of constraining the 3rd-order polynomials to be everywhere zero.

To enforce that the gait model has zero derivative with respect to stride length at zero stride length, we apply a constraint similar to (19), using $\frac{d\Lambda_l}{dl}$ instead of Λ_l:

$$\overbrace{I_4 \otimes \Lambda_{\forall r} \otimes \frac{d\Lambda_l}{dl}(0)}^{\forall B_p, r, \text{ if } l=0,} \otimes \overbrace{\begin{pmatrix} \Lambda_p(0) \\ \Lambda_p(\frac{1}{4}) \\ \Lambda_p(\frac{2}{4}) \\ \Lambda_p(\frac{3}{4}) \end{pmatrix}}^{\forall\ p} \phi \overbrace{\begin{pmatrix} 1 & 0 & 0 \\ 0 & 1 & 0 \\ 0 & 0 & 1 \\ 0 & 0 & 0 \end{pmatrix}}^{\text{ignoring pelvis}} = \overbrace{0_{48\times 3}}^{\text{d/dp=0}}. \quad (20)$$

We also constrain the pelvis to be a linear fit with respect to stride length by constraining it to have a constant derivative with respect to stride length (a constraint similar to (19) with $\frac{d\Lambda_l}{dl}$ instead of Λ_l).

We regressed the model using the constrained least-squares optimization function `lsqlin` in MATLAB (Fig. 1).

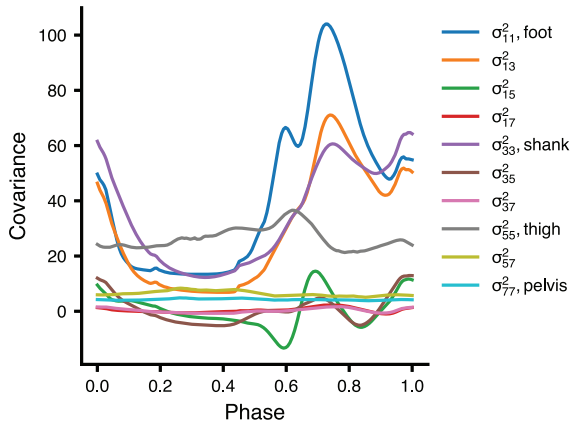

Fig. 2. The heteroscedastic measurement noise model as a function of phase. Foot angle variance σ_{11}, shank angle variance σ_{33}, thigh angle variance σ_{55}, and pelvis angle variance σ_{77}, are shown, along with their respective covariances.

E. Heteroscedastic Noise Model

We developed a heteroscedastic measurement noise model that dynamically changes the measurement noise matrix Σ_R based on phase p. In this schema, Σ_R is defined as

$$\Sigma_R(p) = \Sigma_{R,\text{sensor}} + \Sigma_{R,\text{xsub}}(p), \quad (21)$$

where $\Sigma_{R,\text{sensor}}$ is the traditional measurement noise matrix that denotes how uncertain the measurements are, and $\Sigma_{R,\text{xsub}}$ denotes the uncertainty present due to inter-subject gait kinematic variability (subscript xsub for cross-subject). In this schema, the heteroscedastic model not only encapsulates the uncertainty present due to each person's unique gait, but also can continuously change its trust in the data to capture regions within the gait cycle where the measurements are more trustworthy due to smaller inter-subject gait variability (*e.g.*, flat-foot contact). The matrix $\Sigma_{R,\text{sensor}}$ was set as $\text{diag}[\sigma^2_{11,r}, \sigma^2_{22,r}, \sigma^2_{33,r}, \sigma^2_{44,r}, \sigma^2_{55,r}, \sigma^2_{66,r}, \sigma^2_{77,r}, \sigma^2_{88,r}]$, with each $\sigma_{xx,r}$ representing the standard deviation for $\theta_f, \dot{\theta}_f, \theta_s, \dot{\theta}_s, \theta_t, \dot{\theta}_t, \theta_p, \dot{\theta}_p$, respectively. In our implementation, the $\sigma_{xx,r}$ values that pertained to the angles and angular velocities were set equal to 1 and 10 respectively.

For $\Sigma_{R,\text{xsub}}(p)$ we used the prior dataset to calculate the covariance matrices of the measurement residuals y for the eight measured kinematic variables at each of 150 phase values (Fig. 2). The instantaneous $\Sigma_{R,\text{xsub}}(p)$ was then calculated in real-time using the estimate of phase.

F. Candidate Bayes Filter Implementations

The first filter we tested was the **Ensemble Kalman Filter (EnKF)**, which uses Monte Carlo methods to approximate the state mean and covariance at each time step. This allows for highly nonlinear measurement maps and makes the fewest assumptions of the filters we tested. In the EnKF, these expectations are tracked by N particles $X_k^{(i)}$, $i = 1, \ldots N$, which each evolve through the prediction and update steps of the Kalman Filter. There is a tradeoff between the number of particles used to track the states and the computational times involved in the filter. In our simulations, we use an EnKF with 1000 particles (EnKF1000) and one with 100 particles (EnKF100). In this formulation, each particle is fed through the dynamics and individually corrupted by samples from the process noise. Owing to the requirement that Σ_Q be strictly positive definite (due to directly needing to sample

from the process noise matrix), σ_{11} was set to $1e-20$ to approximate the noiseless integration while maintaining positive definiteness; σ_{22}, σ_{33}, and σ_{44} were set to $1e-2$, $1e-2$, and $1.5e-1$ respectively. State means and covariances were estimated by the empirical means and covariances of the particles $X_k^{(i)}$ (see [40]).

The **Unscented Kalman Filter (UKF)** is capable of approximating the posterior mean and variance of nonlinear functions up to the 3rd order [41]. For the update step of the Kalman Filter, the UKF approximates the mean and covariances of the states using quadrature integration and carefully selected Sigma Points $\mathcal{X}^{[i]}$ and weights $w^{[i]}$. The Sigma Points $\mathcal{X}^{[i]}$ and $w^{[i]}$ were generated using $\alpha = 1e-3$, $\beta = 2$ for the Gaussian approximation, and $\kappa = 0$ according to Wan and van der Merwe [41].

The **Extended Kalman Filter (EKF)** locally linearizes the nonlinear parts of the system (the gait model) for a simple approximation of the normal Kalman Filter. It makes the strongest approximations about the problem, but offers the best computational performance. State means and covariances were updated using the standard linear Gaussian update equations using the Jacobian of h with respect to the gait-state vector x [42].

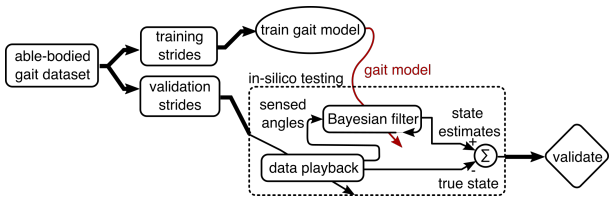

Fig. 3. The Bayesian filter and gait model regression processes. In this cross-validation study, gait data from our dataset is segregated into training strides from non-excluded subjects that are used to regress the gait model, and validation strides from the subject being evaluated. The gait model is then used within each of the four candidate Bayesian filters. The validation strides contain sensor measurements that are input to the Bayesian filter, which then uses the gait model to yield gait state estimates that are compared to the true states from the validation strides.

G. Evaluation of Bayesian Filtering Problems

We evaluated each Kalman Filter with different measurement configurations: 1) full, in which the filter had access to foot, shank, thigh, and pelvis angle data (along with their respective velocities), 2) four configurations in which a different measurement was left out, 3) six configurations in which the different permutations of two measurements from the four kinematics were used (six configurations, *e.g.*, shank-foot, thigh-pelvis), and 4) four configurations in which each filter only had a single respective measurement. For the purposes of abbreviation, the sensors present in each configuration are given by a string composed of the first letter of the angular measurement (foot, shank, thigh, pelvis) aside from the full configuration, which contains all four sensors (*e.g.*, the configuration of shank-foot is 'fs'). For the simulations where angle sensors were dropped from the filtering, the corresponding observation functions were ignored during the filter calculations.

For each combination of filter type and measurement model, we evaluated the combination's gait-state estimation on a simulated walking task that used the data from the same dataset used to regress the gait model. To simulate the filter's performance on unseen subjects, we performed a leave-one-out cross-validation on all ten of the dataset's subjects. For each subject, this cross-validation trained a new gait model and heteroscedastic noise model using the walking data from the remaining nine subjects. The subject's kinematic and walking data were then input to each filter, which estimated the underlying gait-state (Fig. 3). Errors for each of the states at each time point were calculated as the difference between the state estimate and its respective ground truth state measurement from the dataset. This process was repeated for all ten subjects, and the errors were aggregated to obtain overall distributions that described each filter combination's performance in estimating each element of the gait-state. For the EKF, in addition to the configurations above, we evaluated the estimation of limited subsets of the gait-state: 1) a subset where incline was excluded (Cancel Incline), 2) a subset where stride length was excluded (Cancel Stride Length), and 3) a subset where phase and phase rate only where estimated (Phase Only). This simulation was motivated by the potential for limited sensor configurations to still estimate parts of the gait-state vector. Ground truth measurements and state errors were computed as in the simulation with the full gait-state vector. To mitigate the effects of an increasing EKF bandwidth due to the removal of states from the filter, the elements of Σ_Q were scaled in the following way: for Cancel Incline, σ_{33} was scaled by 0.5; for Cancel Stride Length, σ_{44} was scaled by 0.5; for Phase Only, σ_{11} and σ_{22} were scaled by 0.5. To obtain an overall metric for estimation performance, we computed the Mahalanobis distance between the gait-state estimate and the ground truth state at each time point. This Mahalanobis distance was normalized using the average state covariance matrix $\bar{P}_k$ from the full-state, full-measurement EKF simulation; for the simulations where subsets of the gait-state were estimated, we used the subset of $\bar{P}_k$ that corresponded to those gait-states. This error metric captured the overall estimation performance of each combination of gait-state and measurement configuration. We then normalized these errors by the error from the full-state, full-measurement EKF simulation to aid in comparisons.

III. Results

Overall, the Extended Kalman Filter (Fig. 4A) was able to consistently estimate the gait-state despite its restrictive assumptions. With the full measurement configuration, the EKF featured an average phase error of 0.01 ± 0.02 (SD), an average phase rate error of -0.01 ± 0.03 1/s, an average stride length error of 0.03 ± 0.10 m, and an average incline error of 0.08 ± 1.86 degrees. Gait-estimation performance was similar with the UKF (phase: 0.01 ± 0.01, phase rate: -0.01 ± 0.03, stride length: 0.03 ± 0.10, incline: 0.06 ± 1.96), while the EnKF implementations with 1000 particles (phase: 0.03 ± 0.06, phase rate: -0.02 ± 0.05, stride length: 0.03 ± 0.10, incline: 0.16 ± 2.66) and 100 particles (phase: 0.16 ± 0.14, phase rate: -0.06 ± 0.41, stride length: -0.45 ± 0.33, incline: 0.44 ± 7.31) were less reliable.

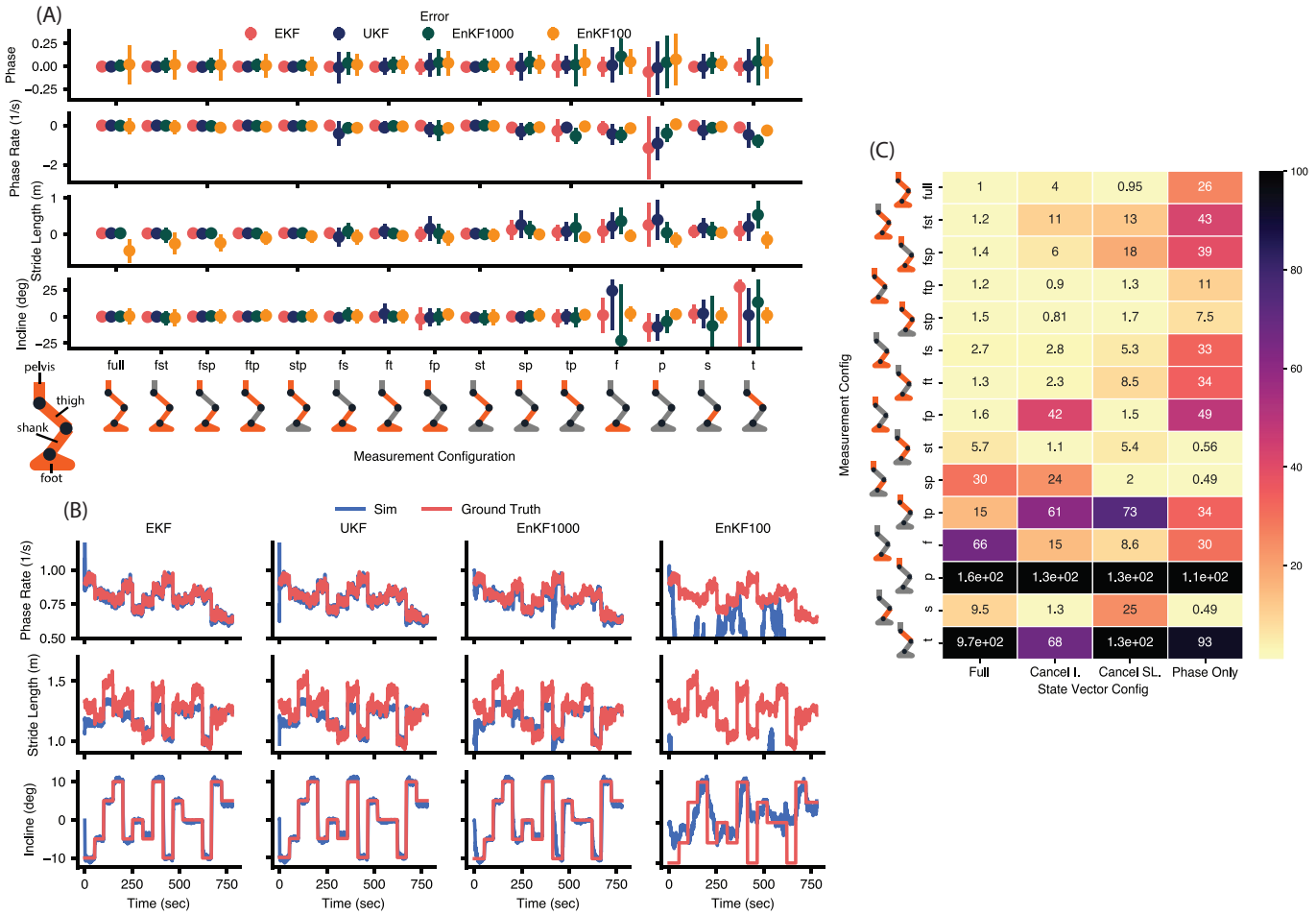

Fig. 4. (A) The errors for all four elements of the gait-state for the four types of Kalman Filter, using each sensor configuration. The means are denoted by the solid circles, with standard deviations given by the vertical lines. Generally speaking, the EKF and UKF provide the best estimation for the four states. For the purposes of abbreviation, the sensors present in each configuration are given by a string composed of the first letter of the angular measurement (foot, shank, thigh, pelvis) aside from the full configuration, which contains all four sensors (*e.g.*, the configuration of shank-foot is 'fs'). (B) Representative results for the three Kalman Filters run in this simulation, with the full sensor configuration. These results were randomly selected from a single subject in the *in silico* cross-validation. The ground truth states are shown in solid red, with the filter estimates shown in blue. Phase is not shown since it is not perceptible at this time scale, but the estimation quality can be inferred from phase rate graphs. (C) EKF estimation performance for the fifteen measurement configurations and four different state vector configurations. Combined state errors were calculated using the Mahalanobis distance weighted by the average state covariance matrix from the baseline case (full sensing, full state, top-left). Errors were then normalized by the error of the baseline state, with higher errors shown in darker colors.

A representative trial of each filter's performance exemplifies these errors (Fig. 4B). For this representative trial, we computed the average root mean square error (RMSE) across all individual strides for each state variable. The EKF (phase RMSE: 0.01 ± 0.009, phase rate RMSE: 0.02 ± 0.02, stride length RMSE: 0.08 ± 0.06, incline RMSE: 0.72 ± 1.62 degrees) was again comparable to the UKF (phase RMSE: 0.01 ± 0.009, phase rate RMSE: 0.02 ± 0.02, stride length RMSE: 0.08 ± 0.06, incline RMSE: 0.73 ± 1.64); the EnKF with 1000 particles (phase RMSE: 0.03 ± 0.06, phase rate RMSE: 0.03 ± 0.04, stride length RMSE: 0.08 ± 0.07, incline RMSE: 1.2 ± 2.5) was also similar, while the EnKF with 100 particles (phase RMSE: 0.15 ± 0.15, phase rate RMSE: 0.27 ± 0.25, stride length RMSE: 0.38 ± 0.21, incline RMSE: 4.95 ± 4.42) was still the poorest estimator.

For the EKF implementation, removing the pelvis or shank measurements did not excessively deteriorate estimation of the full state vector in terms of the normalized Mahalanobis distance metric. In some sparse sensing configurations (s, t, f, sp, st, stp, ftp), gait-state estimation performance was improved by removing either stride length or incline from the state vector (Fig. 4C). Canceling the incline state seemed to be more effective than cancelling stride length, with the exception of sp, f, fp, and the full configuration. The configurations of s, sp, and st were capable of estimating phase accurately without the task variables.

IV. Discussion

Despite being the filter with the weakest assumptions and theoretically best ability to capture the gait-state probability distribution as it evolves through the nonlinear gait model, the EnKFs were overall the worst performing filter based on gait-state errors. In particular, the EnKF with 100 particles (EnKF100) was the worst filter overall, as it featured the highest standard deviations for phase error and incline, and significant biases for stride length error. While increasing the number of particles from 100 to 1000 mitigates these

errors, the EnKF1000 is at best roughly equal to the EKF or UKF. During the simulations, the added complexity in the EnKF1000 led to drastically increased run-times when compared to the EKF and UKF. Taken together, this indicates that the added complexity from an EnKF may be unnecessary for this gait-state estimation task, and instead a simpler EKF or UKF may suffice for the control of an exoskeleton.

The EKF and UKF have close state errors and are thus comparable in performance (Fig. 4A), particularly for the measurement configurations with only a single sensor removed. This has numerous implications for the potential applications of the Bayesian framework to the continuous control of lower-limb wearable robots. For example, the gait model h at the heart of the filters must be linearized in the case of the EKF, which can introduce significant error. However, the EKF performed comparably to the UKF, which can approximate models of up to the third order [41] with more points, and the EnKF, which can more closely approximate the output distributions during the update steps. This indicates that the simple linear approximation of the EKF is sufficient for gait estimation using the gait models developed in this work.

The magnitudes of the phase error from the EKF (0.01 ± 0.02) are comparable to recent methods based on Gaussian Processes [15] (phase RMSE: 0.04 ± 0.005) and machine learning [23], [24] (0.07 ± 0.03 from [23], 0.04 ± 0.006 from [24]), although direct comparison is impossible due to the different testing methods. The EKF incline errors (0.08 ± 1.86 degrees) are also similar to prior work that estimated ground inclination in real-time using machine learning [43] (incline RMSE: $2.15° \pm 0.29°$). As depicted in the representative trial (Fig. 4B) for the EKF, stride length was generally the state with the greatest estimation discrepancy. This error is likely due to the inter-subject gait model being unable to fully distinguish a person's individual gait to better estimate their stride length [18].

In terms of the sensor configurations, predictably, the full sensor array produced the lowest errors. However, some measurement configurations, such as the foot-shank-thigh and foot-shank, have comparable errors to the full configuration, especially for the EKF. Taken together, these results point to the EKF as being the best choice for the gait-state estimation task, and motivated the simulation experiment using the EKF to identify which subsets of the state vector can be estimated using limited sensors. While prior work in gait phase estimation yielded good estimates of phase with thigh angle alone [19], [21], [26], [27], [44], these approaches employed normalization techniques that are not reproduced in our EKF's thigh-only estimation process.

When the measurement vector was limited in simulation, some states were still able to be effectively estimated using the EKF. In terms of the normalized estimation error outlined above, limited sensing configurations such as foot-shank-thigh and foot-thigh are comparable in error to the full-sensing configuration for the full-gait-state case. In particular, the pelvis measurement appears to be the least informative, as configurations with it have similar normalized errors as configurations without. Furthermore, the pelvis sensor alone is easily the worst single measurement across all four gait-state vectors. This suggests that this measurement can be dropped in a practical implementation of the EKF. Conversely, for the most limited case of phase-only state estimation using the EKF, the shank measurement is the optimal choice if only a single measurement is allowed. This indicates that the shank measurement is among the more informative measurements within the EKF framework, and should thus be prioritized in allocating sensors. The overall flexibility of the sensor configuration is a strength of the continuous gait model at the heart of the Kalman Filter. Unlike past methods for estimating the gait-state which required explicit rules to handle new measurements [21], [22], the EKF can incorporate new measurements by simply regressing a relation between the gait-state and the kinematic measurement offline, and then extending the measurement vector in the Kalman Filter. Similarly, the gait state vector can also be extended to include other task variables such as stride height for ascending stairs.

V. Conclusion

We investigated the challenge of estimating gait behavior (phase and task variables) using Bayesian filtering with the sensors available to lower-limb wearable robots. We found this estimation problem to be tractable *in silico*, even with restrictive EKF assumptions and sparse sensing configurations. Our results suggest that an EKF is a good choice for continuously estimating phase and task to drive and adapt an exoskeleton controller. Furthermore, reduced gait-states can be estimated with far fewer measurements using the proposed framework (for example, shank can be used alone if the user wishes to only estimate phase). Future work will involve testing these Kalman Filters on actual exoskeleton hardware, including modular joint configurations [45], to validate them in the real world.

References

[1] L. M. Mooney, E. J. Rouse, and H. M. Herr, "Autonomous exoskeleton reduces metabolic cost of walking," *Conf Proc IEEE Eng Med Biol Soc*, vol. 11, no. 1, pp. 3065–3068, 2014.

[2] J. Zhang, P. Fiers, K. A. Witte, R. W. Jackson, K. L. Poggensee, C. G. Atkeson, and S. H. Collins, "Human-in-the-loop optimization of exoskeleton assistance during walking," *Science*, vol. 1284, no. June, pp. 1280–1284, 2017.

[3] Y. Ding, M. Kim, S. Kuindersma, and C. J. Walsh, "Human-in-the-loop optimization of hip assistance with a soft exosuit during walking," *Science Robotics*, vol. 3, no. 15, pp. 1–9, 2018.

[4] F. A. Panizzolo, G. M. Freisinger, N. Karavas, A. M. Eckert-Erdheim, C. Siviy, A. Long, R. A. Zifchock, M. E. LaFiandra, and C. J. Walsh, "Metabolic cost adaptations during training with a soft exosuit assisting the hip joint," *Sci. Rep.*, vol. 9, no. 1, pp. 1–10, 2019.

[5] G. S. Sawicki, O. N. Beck, I. Kang, and A. J. Young, "The exoskeleton expansion: Improving walking and running economy," *J. NeuroEng. and Rehabilitation*, vol. 17, no. 1, pp. 1–9, 2020.

[6] K. E. Gordon and D. P. Ferris, "Learning to walk with a robotic ankle exoskeleton," *J. biomechanics*, vol. 40, no. 12, pp. 2636–2644, 2007.

[7] T. Lenzi, M. C. Carrozza, and S. K. Agrawal, "Powered hip exoskeletons can reduce the user's hip and ankle muscle activations during walking," *IEEE Trans Neural Syst Rehabil Eng*, vol. 21, no. 6, pp. 938–948, 2013.

[8] H. Zhu, C. Nesler, N. Divekar, V. Peddinti, and R. Gregg, "Design principles for compact, backdrivable actuation in partial-assist powered knee orthoses," *IEEE/ASME Trans. Mechatronics*, 2021.

[9] A. F. Azocar, L. M. Mooney, L. J. Hargrove, and E. J. Rouse, "Design and Characterization of an Open-source Robotic Leg Prosthesis," *Int. Conf. Biomedical Robotics and Biomechatronics*, 2018.

[10] A. J. Young, A. M. Simon, N. P. Fey, and L. J. Hargrove, "Classifying the intent of novel users during human locomotion using powered lower limb prostheses," *Int IEEE EMBS Conf Neural Eng*, pp. 311–314, 2013.

[11] A. J. Young, A. M. Simon, and L. J. Hargrove, "A training method for locomotion mode prediction using powered lower limb prostheses," *IEEE Trans Neural Syst Rehabil Eng*, vol. 22, no. 3, pp. 671–677, 2013.

[12] R. D. Gregg, T. Lenzi, L. J. Hargrove, and J. W. Sensinger, "Virtual constraint control of a powered prosthetic leg: From simulation to experiments with transfemoral amputees," *IEEE Trans. Robotics*, vol. 30, no. 6, pp. 1455–1471, 2014.

[13] H. Huang, F. Zhang, L. J. Hargrove, Z. Dou, D. R. Rogers, and K. B. Englehart, "Continuous locomotion-mode identification for prosthetic legs based on neuromuscular–mechanical fusion," *IEEE Trans. Biomedical Engineering*, vol. 58, no. 10, pp. 2867–2875, 2011.

[14] T. Elery, S. Rezazadeh, C. Nesler, and R. D. Gregg, "Design and validation of a powered knee–ankle prosthesis with high-torque, low-impedance actuators," *IEEE Trans. Robotics*, vol. 36, no. 6, pp. 1649–1668, 2020.

[15] N. Thatte, T. Shah, and H. Geyer, "Robust and adaptive lower limb prosthesis stance control via extended kalman filter-based gait phase estimation," *IEEE Robotics and Automation Letters*, vol. 4, no. 4, pp. 3129–3136, 2019.

[16] R. M. Karulkar and P. M. Wensing, "Using footsteps to estimate changes in the desired gait speed of an exoskeleton user," *IEEE Robot. Autom. Lett.*, vol. 6, no. 4, pp. 6781–6788, 2021.

[17] G. Clark, J. Campbell, S. M. R. Sorkhabadi, W. Zhang, and H. B. Amor, "Predictive modeling of periodic behavior for human-robot symbiotic walking," in *IEEE Int. Conf. Robot. Autom.* IEEE, 2020, pp. 7599–7605.

[18] R. L. Medrano, G. C. Thomas, C. Keais, E. J. Rouse, and R. D. Gregg, "Real-time phase and task estimation for controlling a powered ankle exoskeleton on extremely uneven terrain," *IEEE Trans. Robot.*, 2022, submitted. [Online]. Available: https://web.eecs.umich.edu/locolab/documents/MedranoGregg-TRO2022(submitted).pdf

[19] D. J. Villarreal, H. A. Poonawala, and R. D. Gregg, "A robust parameterization of human gait patterns across phase-shifting perturbations," *IEEE Trans. Neural Syst. Rehabilitation Eng.*, vol. 25, no. 3, pp. 265–278, 2017.

[20] M. A. Holgate, T. G. Sugar, and A. W. Ḃohler, "A novel control algorithm for wearable robotics using phase plane invariants," *IEEE Int. Conf. Robotics and Automation*, pp. 3845–3850, 2009.

[21] D. Quintero, D. J. Villarreal, D. J. Lambert, S. Kapp, and R. D. Gregg, "Continuous-Phase Control of a Powered Knee-Ankle Prosthesis: Amputee Experiments Across Speeds and Inclines," *IEEE Trans. Robotics*, vol. 34, no. 3, pp. 686–701, 2018.

[22] S. Rezazadeh, D. Quintero, N. Divekar, E. Reznick, L. Gray, and R. D. Gregg, "A Phase Variable Approach for Improved Rhythmic and Non-Rhythmic Control of a Powered Knee-Ankle Prosthesis," *IEEE Access*, vol. 7, pp. 109 840–109 855, 2019.

[23] I. Kang, P. Kunapuli, and A. J. Young, "Real-Time Neural Network-Based Gait Phase Estimation Using a Robotic Hip Exoskeleton," *IEEE Trans. Medical Robotics and Bionics*, vol. 2, no. 1, pp. 28–37, 2019.

[24] I. Kang, D. Molinaro, S. Duggal, Y. Chen, P. Kunapuli, and A. Young, "Real-time gait phase estimation for robotic hip exoskeleton control during multimodal locomotion," *IEEE Robotics and Automation Letters*, vol. 6, no. 2, pp. 3491–3497, 2021.

[25] K. Seo, Y. J. Park, J. Lee, S. Hyung, M. Lee, J. Kim, H. Choi, and Y. Shim, "RNN-based on-line continuous gait phase estimation from shank-mounted IMUs to control ankle exoskeletons," *IEEE Int. Conf. Rehabilitation Robotics*, pp. 809–815, 2019.

[26] B. Zhang, M. Zhou, W. Xu *et al.*, "An adaptive framework of real-time continuous gait phase variable estimation for lower-limb wearable robots," *Robotics and Autonomous Systems*, vol. 143, p. 103842, 2021.

[27] W. Hong, N. A. Kumar, and P. Hur, "A phase-shifting based human gait phase estimation for powered transfemoral prostheses," *IEEE Robotics and Automation Letters*, vol. 6, no. 3, pp. 5113–5120, 2021.

[28] M. Shepherd, D. Molinaro, G. Sawicki, and A. Young, "Deep learning enables exoboot control to augment variable-speed walking," *IEEE Robot. Autom. Lett.*, 2022.

[29] M. R. Tucker, J. Olivier, A. Pagel, H. Bleuler, M. Bouri, O. Lambercy, J. del R Millán, R. Riener, H. Vallery, and R. Gassert, "Control strategies for active lower extremity prosthetics and orthotics: a review," *J. Neuroeng. Rehabilitation*, vol. 12, no. 1, 2015.

[30] H. Huang, F. Zhang, L. J. Hargrove, Z. Dou, D. R. Rogers, and K. B. Englehart, "Continuous locomotion-mode identification for prosthetic legs based on neuromuscular-mechanical fusion," *IEEE Trans. Biomedical Engineering*, vol. 58, pp. 2867–2875, 2011.

[31] C. D. Joshi, U. Lahiri, and N. V. Thakor, "Classification of gait phases from lower limb EMG: Application to exoskeleton orthosis," *IEEE Point-of-Care Healthcare Technologies*, pp. 228–231, 2013.

[32] A. J. Young and L. J. Hargrove, "A classification method for user-independent intent recognition for transfemoral amputees using powered lower limb prostheses," *IEEE Trans. Neural Syst. Rehabilitation Eng.*, vol. 24, no. 2, pp. 217–225, 2016.

[33] M. Liu, F. Zhang, and H. H. Huang, "An adaptive classification strategy for reliable locomotion mode recognition," *Sensors*, vol. 17, no. 9, 2017.

[34] B. Hu, A. M. Simon, and L. Hargrove, "Deep generative models with data augmentation to learn robust representations of movement intention for powered leg prostheses," *IEEE Trans. Medical Robotics and Bionics*, vol. 1, no. 4, pp. 267–278, 2019.

[35] W. Choi, W. Yang, J. Na, J. Park, G. Lee, and W. Nam, "Unsupervised gait phase estimation with domain-adversarial neural network and adaptive window," *IEEE J. Biomedical and Health Informatics*, 2021.

[36] K. R. Embry, D. J. Villarreal, R. L. Macaluso, and R. D. Gregg, "Modeling the Kinematics of Human Locomotion over Continuously Varying Speeds and Inclines," *IEEE Trans. Neural Syst. Rehabilitation Eng.*, vol. 26, no. 12, pp. 2342–2350, 2018.

[37] K. R. Embry and R. D. Gregg, "Analysis of continuously varying kinematics for prosthetic leg control applications," *IEEE Trans. Neural Syst. Rehabilitation Eng.*, vol. 29, pp. 262–272, 2021.

[38] T. K. Best, K. R. Embry, E. J. Rouse, and R. D. Gregg, "Phase-variable control of a powered knee-ankle prosthesis over continuously varying speeds and inclines," in *IEEE Int. Conf. Intell. Robots Syst.*, 2021, pp. 6182–6189.

[39] S. Särkkä, *Bayesian filtering and smoothing*. Cambridge University Press, 2013, no. 3.

[40] G. Evensen, "The ensemble kalman filter: Theoretical formulation and practical implementation," *Ocean dynamics*, vol. 53, no. 4, pp. 343–367, 2003.

[41] E. A. Wan and R. Van Der Merwe, "The unscented kalman filter for nonlinear estimation," in *IEEE Adaptive Systems for Signal Processing, Communications, and Control Symposium (Cat. No. 00EX373)*, 2000, pp. 153–158.

[42] S. J. Julier and J. K. Uhlmann, "Unscented filtering and nonlinear estimation," *Proc. IEEE*, vol. 92, no. 3, pp. 401–422, 2004.

[43] D. Lee, I. Kang, D. D. Molinaro, A. Yu, and A. J. Young, "Real-time user-independent slope prediction using deep learning for modulation of robotic knee exoskeleton assistance," *IEEE Robot. Autom. Lett.*, 2021.

[44] R. Macaluso, K. Embry, D. J. Villarreal, and R. D. Gregg, "Parameterizing human locomotion across quasi-random treadmill perturbations and inclines," *IEEE Trans. Neural Syst. Rehabilitation Eng.*, vol. 29, pp. 508–516, 2021.

[45] C. Nesler, G. Thomas, N. Divekar, E. Rouse, and R. D. Gregg, "Enhancing voluntary motion with modular, backdrivable, powered hip and knee orthoses," *IEEE Robot. Autom. Lett.*, 2022.